Lestinen, Sami; Kilpeläinen, Simo; Kosonen, Risto; Jokisalo, Juha; Koskela, Hannu

Experimental study on airflow characteristics with asymmetrical heat load distribution and low-momentum diffuse ceiling ventilation

Published in:
Building and Environment

DOI:
10.1016/j.buildenv.2018.02.029

Published: 15/04/2018

Document Version
Peer-reviewed accepted author manuscript, also known as Final accepted manuscript or Post-print

Experimental study on airflow characteristics with asymmetrical heat load distribution and low-momentum diffuse ceiling ventilation

Sami Lestinen[1,*], Simo Kilpeläinen[1], Risto Kosonen[1], Juha Jokisalo[1], Hannu Koskela[2]

[1] Aalto University, School of Engineering, Department of Mechanical Engineering, Sähkömiehentie 4, 02150 Espoo, Finland

[2] Turku University of Applied Sciences, Lemminkäisenkatu 14-18 B, FI-20520 Turku, Finland

*corresponding author: sami.lestinen@aalto.fi

Abstract

Airflow characteristics were studied with asymmetrically distributed heat load and diffuse ceiling ventilation. The heat load was gradually increased from 40 to 80 W/floor-m^2 while the target temperature of exhaust air was kept at 26±0.5°C. Experiments were carried out in a test room by conducting measurements with omnidirectional anemometers, data loggers and marker-smoke visualizations. The heat load consisted of two opposite workstations next to heated window panels in the perimeter area. The other side of the room was an open area describing a corridor zone. The workstation had a seated test dummy with laptop and monitor. The results indicate that asymmetrical heat load distribution creates a large-scale circulating airflow pattern from the heat sources to the opposite side of the room. Furthermore, the mean air speed and the airflow fluctuation increased with heat load and supply airflow rate. Consequently, also the turbulent kinetic energy and the turbulence dissipation increased. However, heat load had only a small effect on the turbulence intensity and the fluctuation energy ratio. Therefore, draught rate increased significantly with mean air speed. The observed results agree mainly with the symmetrical results otherwise, except for the systematic large-scale circulation that was not found in the symmetrical test case. The maximum draught rate was 18-21 % indicating the category B-C of thermal

environment defined by the European Standard EN ISO 7730:2005. The thermal conditions at the investigated heat loads of 40-80 W/floor-m^2 were not able to fulfill the category A.

Keywords: airflow characteristics, asymmetrical heat load, buoyancy flows, air distribution, Fourier analysis, airflow interaction

Nomenclature

f	frequency [Hz]
i, j, k	index notation of components
k_t	turbulent kinetic energy [m^2/s^2]
l	length scale [m]
N	discrete data set
$S(f)$	power spectral density [m^2/s^2]
t	time [s]
$t_{a,l}$	local air temperature [°C]
Tu	turbulence intensity [%]
U	air speed [m/s]
$\overline{U}$	mean air speed [m/s]
U'	fluctuating component of air speed [m/s]
ε	dissipation [m^2/s^3]
ν	kinematic viscosity [m^2/s]
τ_l	time scale for largest length scales

v_η, l_η, τ_η	Kolmogorov velocity, length and time scale [m/s], [m], [s]
ϕ	variable
$\hat{\phi}(f)_k$	discrete Fourier transform
CCMV	chilled-ceiling with mixing-ventilation system
CBR	chilled-beam with radiant-panel system
MVRC	local radiant cooling panels with mixing-ventilation
DCV	diffuse-ceiling ventilation

1 Introduction

Earlier studies have shown that ventilation is essential for good indoor environmental quality (IEQ) [1] - [3], which, in turn, has been shown to affect significantly on performance and learning [4], [5]. The air distribution is thereby a major factor for health, comfort and performance [6]. Probably the main challenge in air distribution is to produce clean air for individuals, maintain thermal conditions, and reduce pollutants from a breathing zone. In large enclosures, occupied zones covered typically only a small volume compared with total space volume [7], [8]. In offices, the main challenge has been to distribute clean air to workstations without draught risk and to optimize thermal environment. In this sense, advanced air distribution methods play a major role in responding to spatial and temporal changes in user-centric environments.

One of the advanced air distribution methods is a diffuse ceiling ventilation, in which the low-momentum supply air is distributed evenly through the perforated ceiling down to the occupied zone [9], [10]. This means that when the low-momentum ventilation is introduced, the heat load controls the airflow patterns [11]. In principle, this air distribution method can handle high internal

heat loads and improve thermal comfort in the occupied zone [12] - [14]. However, thermal load distribution and ceiling height may affect a performance of diffuse ceiling ventilation [11].

Generally, controlling room airflows can be very difficult in the occupied zone [15]. The ventilation jets and the buoyancy flows may form a complicated airflow field involving changes that are difficult to predict. Therefore, it is not a surprise that thermal discomfort has been a common complaint in the offices [16] - [18]. For instance, the risk of draught increases when the airflow temperature decreases and the mean velocity and the turbulence intensity increase [19]. Hence, the airflow patterns have a significant effect on satisfaction with thermal environments.

The room airflow pattern depends on the heat source strength and relative locations of air distribution units and heat sources [20] - [22]. A thermal plume grows up from a heat source that is warmer than a surrounding air. The air is heated which creates a density difference and the buoyancy force accelerates the plume upwards due to gravity. Consequently, temperature gradients are created and energy is transported throughout the room interacting with the velocity field [23]. A plume decays gradually when the temperature gradient vanishes and the surrounding air entrains to the flow due to viscous forces and static pressure differences.

Indoor airflows are mainly turbulent at increased heat load conditions. Turbulence is chaotic and random flow motion that involves a wide range of scales [24] - [26]. Turbulent kinetic energy is transferred from the energy of the mean flow to the largest eddies from where it is further transferred to the smaller and still smaller eddies until the energy is dissipated into heat. This process is usually fast, thus the transfer occurs within short distance. Turbulence increases the transport of energy, but requires continuous supply of energy against the turbulent stresses [27]. Consequently, turbulence may have a significant effect on airflow characteristics.

This study investigates averaged airflow characteristics [28] - [30] with a low-momentum ceiling air distribution and an asymmetrical set-up of heat sources. The motivation is to continue discussion that earlier studies have contributed to the airflow characteristics in indoor environments. For instance, the asymmetrical heat load distribution has been found to provide a large-scale circulating airflow pattern in the room [20], [31]. The objectives of this study were to characterize a

time and a spatial averaged airflow field and to observe airflow fluctuation in an occupied zone under increasing heat load conditions. Consequently, the airflow characteristics form a physical basis for investigating the dependencies, regularities and relationships in indoor air e.g. when optimizing airflow conditions. In addition, this experimental set-up offers a good platform for exploring buoyancy flows and their effects on surroundings.

Novelty of the study comes from systematic investigation and detailed analysis of time and spatial averaged quantities and functions that are focused on the seated person zone. Furthermore, the asymmetrical heat load results are compared to the symmetrical heat load results [32], and also to the experiments with advanced air distribution systems [33]. The airflow characteristics are discussed including turbulent kinetic energy, fluctuation energy and turbulence scales in the flow. The additional characteristics are based on the flow properties and functions describing viscous fluid flow. A seated test dummy was used to model a human heat source at the workstation, because the test dummy has been found to model a sitting person properly [34].

2 Methods

2.1 Test room

The measurements were carried out in a test room of internal dimensions of 5.5 m length, 3.8 m width and 3.2 m height. The test room was located inside a laboratory hall such that outer environment was stable. The floor area was around 21 m^2. The air distribution was introduced by discharging supply air through the entire ceiling surface down to the occupied zone. The depth of suspended ceiling was 0.35 m forming the upper plenum chamber. The suspended ceiling was made of perforated glass wool elements. The degree of perforation was 0.50±0.02%. The diameter of supply air nozzles at the ceiling was 14 mm. The nozzle row next to each wall was sealed. The indoor air was extracted at the suspended ceiling at height 3.2 m. The diameter of the exhaust duct was 0.16 m.

2.2 Experimental set-up

The double office layout and the measurement locations 1-15 are shown in Figure 1.

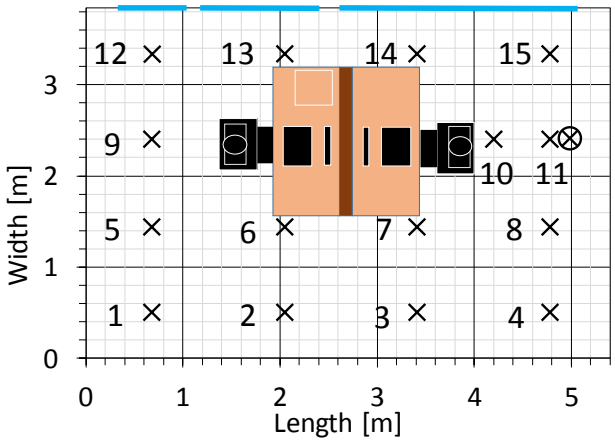

Figure 1. A top-view of measurement locations 1-15 and the double office layout next to the heated window panels in the side-wall (bold lines, width-coordinate 3.84 m). The exhaust air opening is at the ceiling (circle, length-coordinate 5 m, width-coordinate 2.4 m). The additional heat source is under the table (square, length-coordinate 2.4 m, width-coordinate 3 m).

The flow field was measured with seven omnidirectional anemometers. The anemometers were installed at the heights of 0.1 m, 0.6 m, 1.1 m, 1.4 m, 1.7 m, 2.3 m and 2.9 m in accordance with the recommendations in the standard EN ISO 7726:2001 [35]. Three lowest sensors were the Vivo Draught 20T31 anemometers [36] with the sampling rate of 10 Hz. The four highest sensors were the wireless Sensoanemo 5100SF anemometers [37] with the sampling rate of 0.5 Hz. The averaging interval was 1 h. The Tinytagplus-2 data loggers [38] were installed on the internal and on the outer walls to observe near-wall temperature conditions. The detailed temperature differences at surfaces were measured with infrared camera and with infrared thermometer.

Figure 2 shows the test room and the workstation set-up. Two workstations were located 0.6 m from the window panels in the middle of the room in longwise direction. A light was installed at the ceiling in the middle of the workstations at height 3.2 m. A laptop and a monitor were located on

both tables. A partition wall of the height of 1.46 m was installed between the tables. In the case of 80 W/floor-m^2, the additional heat source of 0.4 x 0.4 x 0.4 m^3 was located on the floor below the table to model a computer at the length-coordinate of 2.4 m and the width-coordinate of 2.8 m (Figure 1).

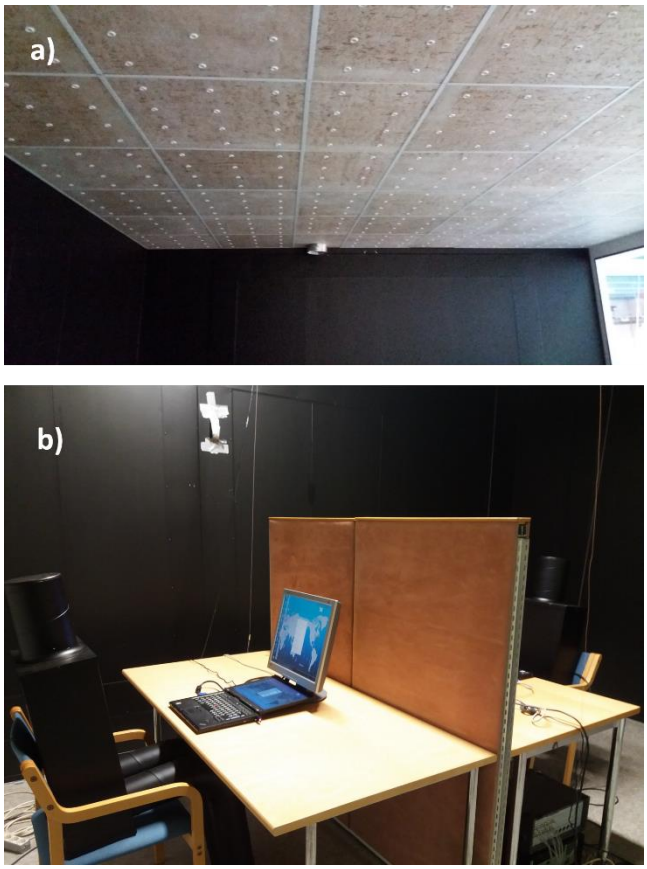

Figure 2. Test room and workstation set-up: a) The suspended ceiling with the degree of perforation of 0.50±0.02 % and b) a seated dummy with a laptop and a monitor near the heated window-panels.

The window panel surface was set to 30-40°C such that the target heat load was achieved. The heating power was provided by conducting hot-water pipes inside the panel. The insulation plates of the thickness of 0.1 m were installed outside the room to cover the window panels. Heating foil of 5 m length and 1 m width was installed on the floor 0.8 m from the heated window panel wall. The heat load of window panels was measured from the water mass-flow and temperature difference between the water supply and return. Furthermore, the heat load was estimated from

the window panel surfaces inside the room. The indoor airflow patterns were visualized with marker smoke. Table 1 shows the test cases and Table 2 summarizes the measuring instruments.

Table 1. The initial data of the test cases. The floor area is 21 m^2.

Test case	**40**	**60**	**80**
Heat load [W/floor-m^2]	40±2	57±3	80±4
Exhaust air temp [°C]	26±0.5	26±0.5	26±0.5
Supply air [l/s,m^2]	3.6±0.2	5.2±0.3	7.3±0.4
Supply air temp [°C]	17±0.2	17±0.2	17±0.2
2 x Dummy [W]	176±9	176±9	176±9
2 x Laptop [W]	96±5	96±5	96±5
2 x Monitor [W]	70±4	70±4	70±4
Computer at floor [W]	0	0	103±5
Light [W]	116±6	116±6	116±6
7 x Window panel [W]	381±19	317±16	696±35
Solar load at floor [W]	0	420±21	420±21

Table 2. The measuring instruments.

Variable	**Meter-type**	**Model**	**Accuracy**
Air temperature Air speed (at height 0.1 m-1.1 m)	Omnidirectional anemometer	Dantec dynamics Vivo Draught 20T31	Air speed (v): range 0.05-1.0 m/s ±0.01 m/s±0.025·v_{meas} Temperature (t): range 0-45°C ±0.15°C Sampling rate 10 Hz STDerr < 10 % upto 2 Hz, time-constant < 0.1 s (v) time-constant < 1 s (t)
Air temperature Air speed (at height 1.4 m-2.9 m)	Omnidirectional anemometer	Sensor electronic SensoAnemo 5100SF	Air speed (v): Range 0.05-5 m/s ±0.02 m/s±0.015 v_{meas} Temperature (t): Range −10-50°C ±0.2°C Sampling rate 8 Hz STDerr<10 % upto 1.5 Hz 90 % response time < 0.2 s
Air temperature	Tinytag data logger	Tinytagplus-2	±0.5°C (0…+45°C)
Surface temperature	Infrared camera	ThermaCAM™ P60	±2°C or ±2% of reading

Surface temperature	Infrared thermometer	Testo 860-T1	±1°C or ±1% of reading
Pressure difference	Measuring instrument	Swema 3000	±0.3% of reading, lowest ±0.3Pa
Airflow rate	Regulation and measuring device	IRIS-200	±5%

2.3 Airflow characteristics

The Standard EN ISO 7730:2005 [19] defines the draught rate as

$$DR = \left(34 - t_{a,l}\right)\left(\overline{U}_{a,l} - 0.05\right)^{0.62}\left(0.37 \cdot \overline{U}_{a,l} \cdot Tu + 3.14\right) \quad (1)$$

The turbulence intensity is expressed as

$$Tu = \frac{U_{sd}}{\overline{U}} \times 100 \ [\%] \quad (2)$$

The turbulent kinetic energy is determined for omnidirectional measurements [28] as

$$k_t = \frac{1}{2}\overline{U'U'} \quad (3)$$

The Discrete Fourier transform was calculated using Matlab R2017 software [39] defined as

$$\hat{\phi}(f)_k = \sum_{j=1}^{N} \phi(t)_j e^{(-2\pi i(j-1)(k-1)/N)} \quad (4)$$

Furthermore, the power spectral density is determined as

$$S(f) = \frac{1}{N}\left|\hat{\phi}(f)\right|^2 \quad (5)$$

The fluctuation energy ratio for a time-series record is defined as

$$\mathrm{X}(E) = \frac{\sum_{i=1}^{N}(U'U')_i \, \Delta t_i}{\sum_{i=1}^{N}(UU)_i \, \Delta t_i} \quad (6)$$

that shows an amount of fluctuation energy over the inertial energy including the mean airflow motion [32]. The Kolmogorov scales [40], [41] are expressed as

$$v_\eta = (\nu\varepsilon)^{1/4} \;;\; l_\eta = \left(\frac{\nu^3}{\varepsilon}\right)^{1/4} \;;\; \tau_\eta = \left(\frac{\nu}{\varepsilon}\right)^{1/2} \tag{7}$$

The time-scale is defined as a ratio of length scale to mean air speed as

$$\tau_l \sim \frac{l}{\overline{U}} \tag{8}$$

The relationship between turbulent kinetic energy and turbulence dissipation is approximated [41], [42] as

$$\varepsilon \sim \frac{{k_t}^{3/2}}{l} \tag{9}$$

The absolute expanded uncertainty at 95% confidence interval can be determined for anemometers [43]. The minimum realistic uncertainty of measuring mean air speed $\overline{U}$ is expressed as

$$d\overline{U} = 0.025 + 0.025 \cdot \overline{U} \tag{10}$$

The corresponding uncertainty for the standard deviation of air speed measurement U_{sd} can be defined as

$$dU_{sd} = 0.007 + 0.15 \cdot U_{sd} \tag{11}$$

The minimum realistic uncertainty for the turbulence intensity is determined as

$$dTu = 4 + 0.23 \cdot Tu\ [\%] \tag{12}$$

A realistic uncertainty for the draught rate *DR* has been estimated to be ±5 % [43].

3 Results

3.1 Temperature

Figure 3 shows the average temperature distribution and statistics in the room with the heat load of 40-80 W/floor-m^2. The arithmetic average of all the measured mean temperatures was 25.8±0.4°C (±std), where the parenthesis refers to ±standard deviation. Consequently, the experiments agree mainly with the target level of 26±0.5°C in the exhaust air. The vertical air temperature difference was small, i.e. the average temperature increased 0.3°C in the seated person zone from the height of 0.1 m to 1.1 m and decreased 0.3°C in the upper zone from the height of 1.4 m to 2.9 m with respect to the test cases 40-80 W/floor-m^2.

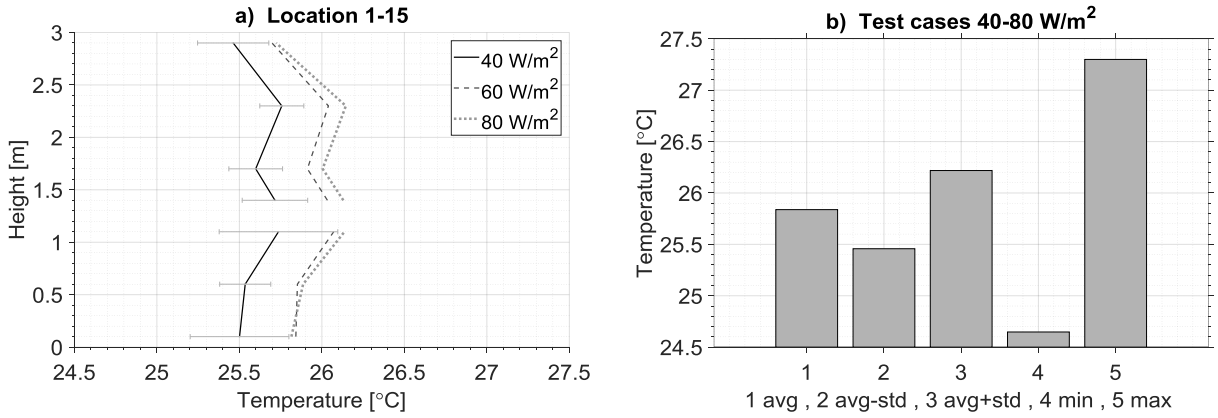

Figure 3. a) The average air temperature in the locations 1-15 (Figure 1) at the heat load of 40-80 W/floor-m^2. The errorbars denote ±standard deviation at 40 W/floor-m^2. b) The corresponding air temperature statistics in the test cases 40-80 W/floor-m^2.

Figure 4 shows air temperature at the corridor side, in the middle and at the window side. In the seated person zone, the average temperature difference from the heated window side to the corridor side was 0.5°C in the case of 40 W/m^2 that was larger than the minimum realistic uncertainty of the measurement (±0.2°C). The corresponding average difference was 0.9°C in the case of 80 W/m^2, thus below 4 % relative difference was obtained. For instance, Mustakallio et al. (2016) [33] showed a smaller temperature range at the heat load of 38 W/m^2 with a chilled-beam with radiant-panel (CBR) system and a chilled-ceiling with mixing-ventilation (CCMV) system than the current study with a diffuse ceiling ventilation (DCV) system at 40 W/m^2. However, a larger

temperature range was found with those systems at the heat load of 64 W/m^2 than in the present study at 60 W/m^2. Furthermore, the authors found a greater temperature difference between the heated-side and the corridor-side at the height of 1.1 m than the current study. However, the air temperature was at a reasonable level in all those test cases. The observed results agree mainly with the earlier study on symmetrical heat-load set-up [32] otherwise, except for the temperature distribution that was more uniform in the test room with symmetrical set-up.

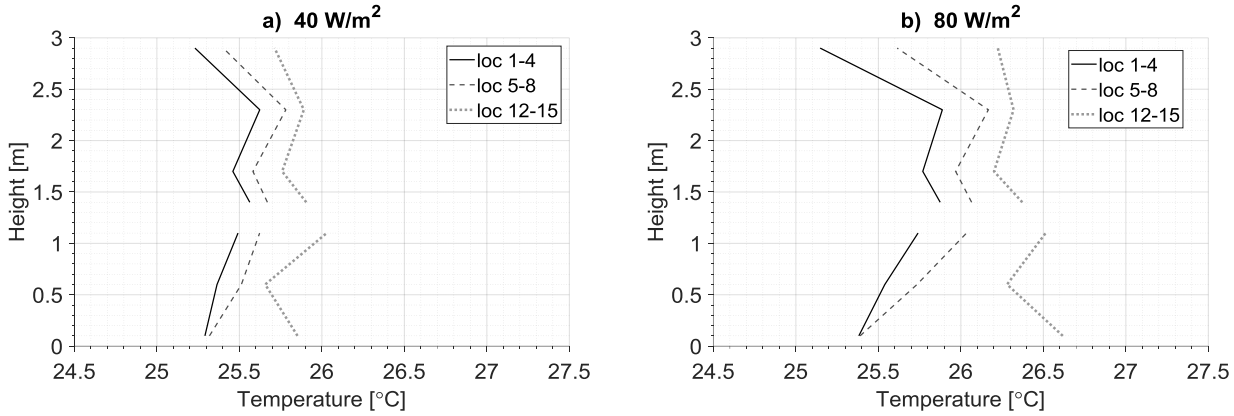

Figure 4. The mean air temperature at the corridor side (location 1-4), in the middle (location 5-8) and at the window side (location12-15): a) the case of 40 W/m^2, b) the case of 80 W/m^2.

3.2 Mean air speed

Figure 5 shows the mean air speed with increasing heat load. The arithmetic average of mean air speeds was 0.11±0.04 m/s (±std) at 40 W/m^2. The corresponding mean air speed increased on average by 31 % up to 0.14±0.06 m/s at 80 W/m^2. Hence, the heat load had a significant effect on air speed level, similarly as in the symmetrical heat load study [32]. However, supply airflow rate also affects on the result. The average mean air speed was 0.14±0.06 m/s below the height of 1.1 m that refers to a seated person zone. Furthermore, the observed mean air speed decreased on average by 19 % from the seated person zone to the upper zone that was defined as a height of 1.4-2.9 m. In the seated person zone, the mean air speed of 0.18±0.07 m/s decreased on average by 42 % down to 0.11±0.04 m/s from the height of 0.1 m up to 1.1 m, respectively. The uncertainty of measurement was ±0.03 m/s as defined by Eq. (10). The largest vertical gradients on air speed

occurred not only in the seated person zone but also near the ceiling zone. Consequently, the highest mean air speed of 0.32 m/s was observed at the height of 0.1 m and 0.23 m/s at the height of 2.9 m with the heat load of 80 W/m^2 and 60 W/m^2, respectively.

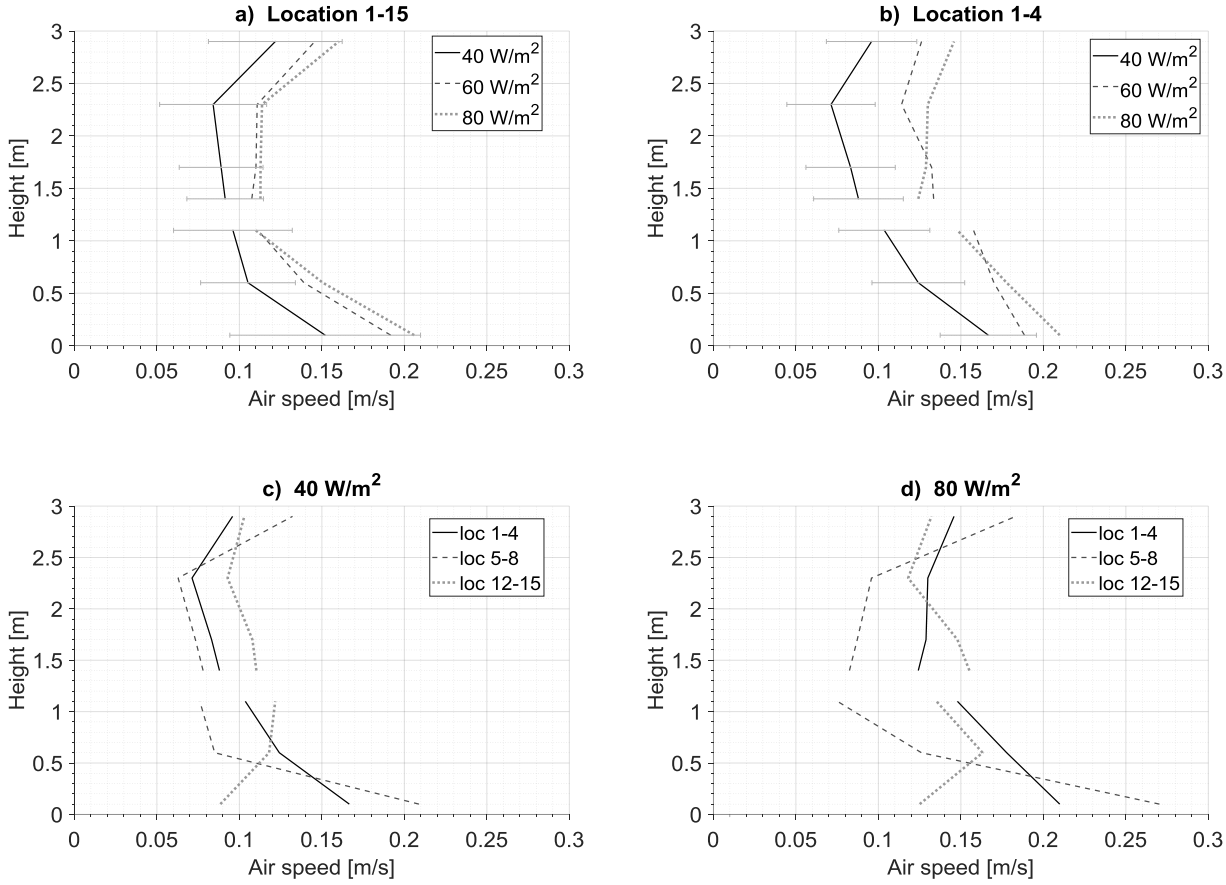

Figure 5. The mean air speed as a function of room height and at the heat load of 40-80 W/m^2: a) Arithmetic average of measured locations 1-15, the errorbars denote ±standard deviation at 40 W/m^2. b) Arithmetic average at the corridor side (location 1-4), the errorbars denote ±uncertainty of measurement at 40 W/m^2 defined by Eq. (10). c) The mean air speed at the corridor side (loc. 1-4), in the middle (loc. 5-8) and at the window side (loc.12-15) in the case of 40 W/m^2 and d) in the case of 80 W/m^2.

In the case of 40 W/m^2, the average mean air speed was 0.11±0.02 m/s at the window side and it increased 20 % up to 0.13±0.04 m/s to the corridor side while the seated person zone was investigated. In the case of 80 W/m^2, the corresponding increase was 26 % from 0.14±0.03 m/s to 0.18±0.05 m/s, respectively.

At the corridor side (locations 1-4), the average mean air speed of 0.13 m/s in the lower zone increased by 36 % up to 0.18 m/s while the heat load was increased from 40 W/m^2 to 80 W/m^2. The corresponding increase was on average 29 % from 0.11 m/s to 0.14 m/s at the window side (locations 12-15), respectively. Hence, the air speed level was lower at the window side than at the corridor side. However, the largest and the smallest air speeds were found in the middle of the room at the locations 5-8 (Figure 5cd).

A marker smoke visualization showed a systematic large-scale circulating airflow pattern from the heat-sources to the other side of the room. Such a circulation was not found with the symmetrical heat load distribution [32]. The observed large-scale circulation follows closely the findings in the earlier studies [21] - [22]. Furthermore, Mustakallio et al. [33] found similar mean air speed levels for both the chilled-beam with radiant-panel system (CBR) and for the chilled-ceiling with mixing-ventilation system (CCMV) than the current study at 40 W/m^2. However, the mean air speed was even 46 % smaller for the local radiant-cooling panels with mixing-ventilation (MVRC) correspondingly.

3.3 Turbulence intensity

Figure 6 shows the turbulence intensity defined by Eq. (2) with the asymmetrical heat load set-up in the seated person zone. In this zone, the arithmetic average of turbulence intensity was 45±15 % (p.p.) in the case of 40 W/m^2. The corresponding level was 44±16% (p.p.) at 80 W/m^2, hence the average turbulence intensity decreased only by 3% towards the increasing heat load. In the symmetrical heat load study [32], the corresponding relative difference was 10 %. This small effect occurred apparently because both the mean air speed and the standard deviation increased with the heat load and the supply airflow rate. The uncertainty of measurement was 14±4 % (±std) in the cases of 40 W/m^2 and 80 W/m^2 as defined by Eq. (12). The average turbulence intensity was at the same level than with the advanced cooling systems studied by Mustakallio et al. [33].

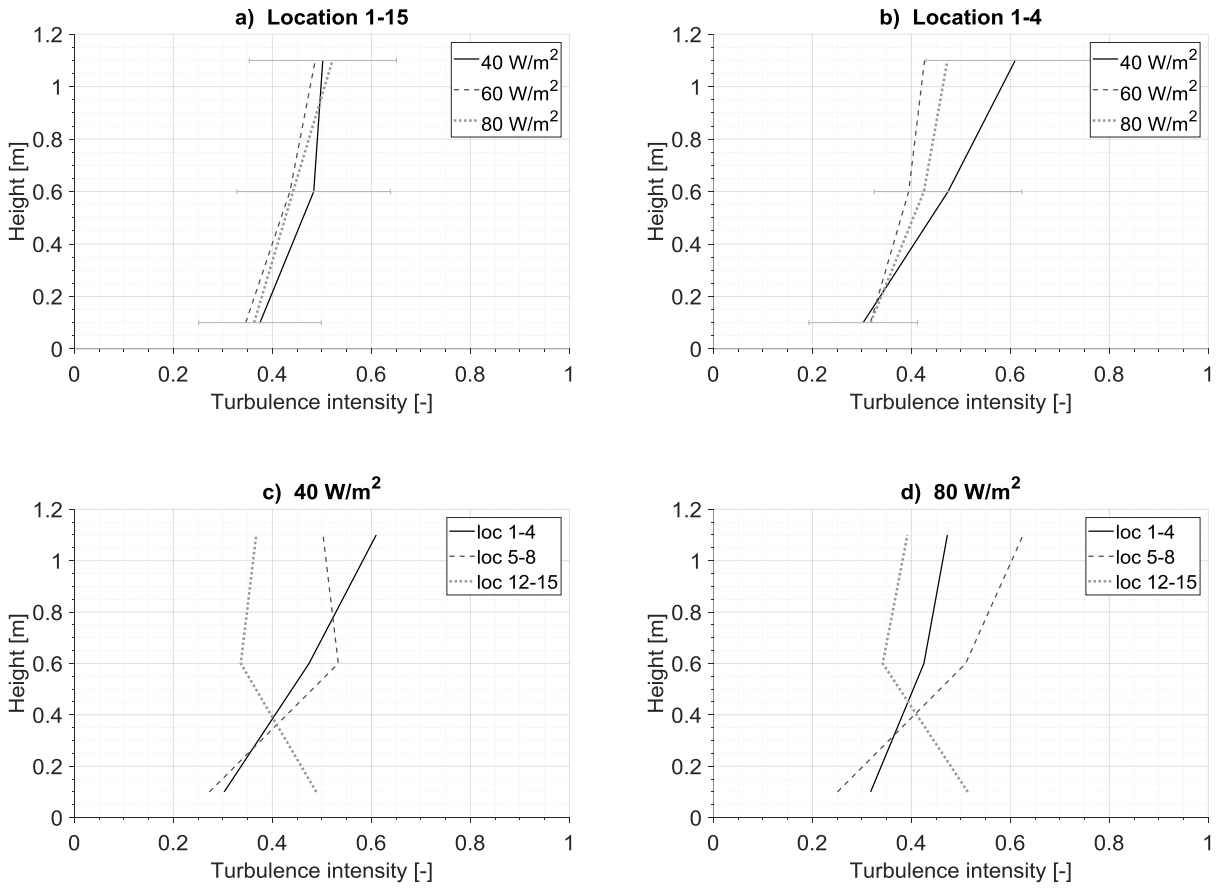

Figure 6. Turbulence intensity as a function of room height in the seated person zone at the heat load of 40-80 W/m^2: a) Arithmetic average of measured locations 1-15 and ±standard deviation at 40 W/m^2. b) Arithmetic average of locations 1-4, i.e. at the corridor side, and ±uncertainty of measurement at 40 W/m^2 defined by Eq. (12). c) Turbulence intensity at the corridor side (loc. 1-4), in the middle (loc. 5-8) and at the window side (loc.12-15) in the case of 40 W/m^2 and d) in the case of 80 W/m^2.

In the seated person zone, the average turbulence intensity of 36±13 % (p.p.) at the height of 0.1 m increased on average by 39 % up to 50±14 % (p.p.) at the height of 1.1 m, mainly because the air speed level was low at 1.1 m in each case, i.e. at the head level of a sitting person. Consequently, a greater effect on turbulence intensity was obtained with the prevailing mean air speed level than with the heat load level. This is mainly because a portion of airflow fluctuation may increase significantly towards lower air speed levels.

In the case of 40 W/m^2, the average turbulence intensity of 40±9 % (p.p.) at the window side increased by 16 % up to 46±16 % (p.p.) at the corridor-side when the seated person zone was investigated. This indicates rather similar airflow fluctuation in the both sides of the room. In the case of 80 W/m^2, the corresponding turbulence intensity was 42±9 % (p.p.) and 41±11 % (p.p.), respectively. This also indicates a small effect of heat load change on the turbulence intensity.

3.4 Draught rate

Figure 7 shows the increase of draught rate defined by Eq. (1) in the seated person zone. In this zone, the arithmetic average of draught rate was 7.5±4.0 % (p.p.) at 40 W/m^2. The corresponding draught rate was 10.4±5.5 % (p.p.) at 80 W/m^2, hence the average draught rate increased by 39% with the heat load. Consequently, the relative effect was only slightly greater than with the mean air speed, but much greater than with the turbulence intensity. Furthermore, the maximum draught rate was 18 % and 21 % at 40 W/m^2 and 80 W/m^2 in the seated person zone, respectively.

In the symmetrical set-up [32], the average draught rate was larger than in the asymmetrical set-up. However, the maximum in the symmetrical set-up was lower at 40 W/m^2 and at the same level at 80 W/m^2 than in the asymmetrical set-up. Mustakallio et al. (2016) [33] found rather similar average draught rates with CCMV and CBR compared to present study with DCV. However, MVRC provided much smaller average draught rate than the current study. Furthermore, the given draught rates were generally small and the differences were mainly within the uncertainty of measurement (±5 % p.p.). Although the average draught rates were below 10% in those test cases, the local maximum was 10-20 % with CCMV, CBR and DCV at the usual heat load conditions (38-40 W/m^2) and at the design heat load conditions (57-64 W/m^2) indicating the category B defined by the European Standard EN ISO 7730:2005 [19]. An exception was MVRC, which provided below 10 % maximum at 38 W/m^2, thus indicating the category A at the usual heat load conditions. However, uncertainty of measurements provides also uncertainty in classification, correspondingly.

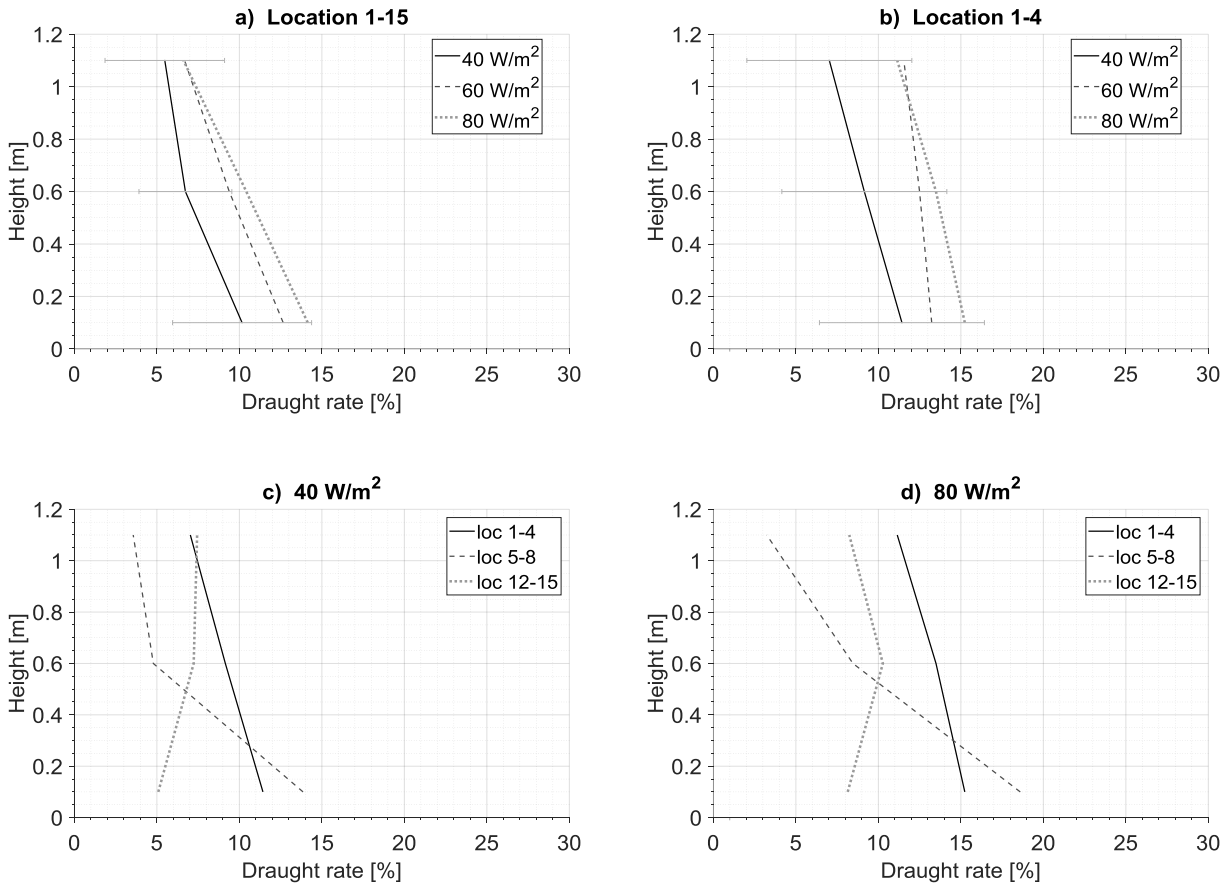

Figure 7. Draught rate as a function of room height in the seated person zone at the heat load of 40-80 W/m^2: a) Arithmetic average of measured locations 1-15 and ±standard deviation at 40 W/m^2. b) Arithmetic average of locations 1-4, i.e. at the corridor side, and ±uncertainty of measurement (±5 % p.p.) at 40 W/m^2 [43]. c) Draught rate at the corridor side (loc. 1-4), in the middle (loc. 5-8) and at the window side (loc.12-15) in the case of 40 W/m^2 and d) in the case of 80 W/m^2.

In this study, the highest draught rate was obtained near the floor, similarly to the symmetrical heat load set-up [32]. This is mainly because the mean air speed was largest near the floor. While considering the seated person zone, the average draught rate of 12.3±4.9 % (p.p.) at the height of 0.1 m decreased by 49 % down to 6.3±4.2 % (p.p.) at the height of 1.1 m, obviously because the mean air speed was low at 1.1 m. In the symmetrical set-up, those average draught rates were slightly greater, but the relative difference was at the same level i.e. 45 % than in the current study.

In the case of 40 W/m^2, the average draught rate of 6.6±1.7 % (p.p.) at the window side increased by 40 % up to 9.2±3.6 % (p.p.) at the corridor-side when the seated person zone was investigated. This indicates smaller draught risk level near the heat sources than in the other side of the room. However, heat sources generate also thermal radiation that affects satisfaction with thermal environment. In addition, the average draught rates were generally at a low level and the average difference between the window side and the corridor side was within uncertainty of measurement. In the case of 80 W/m^2, the draught rate of 8.9±2.0 % (p.p.) at the window side increased on average by 50 % up to 13.3±3.8 % (p.p.) at the corridor side, correspondingly. This indicates greater draught rate level with increased heat load and greater draught rate level in the other side of the room.

At the corridor side (locations 1-4), the average draught rate of 9.2 % (p.p.) increased by 44 % up to 13.3 % (p.p.) while the heat load was increased from 40 W/m^2 to 80 W/m^2. At the window side (locations 12-15), the corresponding draught rate of 6.6 % (p.p.) increased by 35 % up to 8.9 % (p.p.). The relative effect was greater than with the mean air speed and much greater than with the turbulence intensity.

3.5 Air speed fluctuation

Figure 8 shows the increase of air speed fluctuation with heat load in the seated person zone. In this zone, the arithmetic average of the standard deviations of the instantaneous air speed records (1 h) was 0.05 m/s in the case of 40 W/m^2. The corresponding standard deviation was 0.06 m/s at 80 W/m^2, hence the average standard deviation increased by 24% from the heat load of 40 W/m^2 to 80 W/m^2. Consequently, the relative effect was smaller than with the mean air speed but larger than with the turbulence intensity. The uncertainty of measurement was less than ±0.02 m/s as defined by Eq. (11). Furthermore, the average air speed fluctuation was 41 % and 38 % over the mean air speed, respectively. This means that a portion of fluctuation with respect to mean air speed was almost at the same level in both cases. In the symmetrical heat load set-up [32], the

average standard deviations were higher and the portion of fluctuation over the mean air speed was greater than in the asymmetrical set-up.

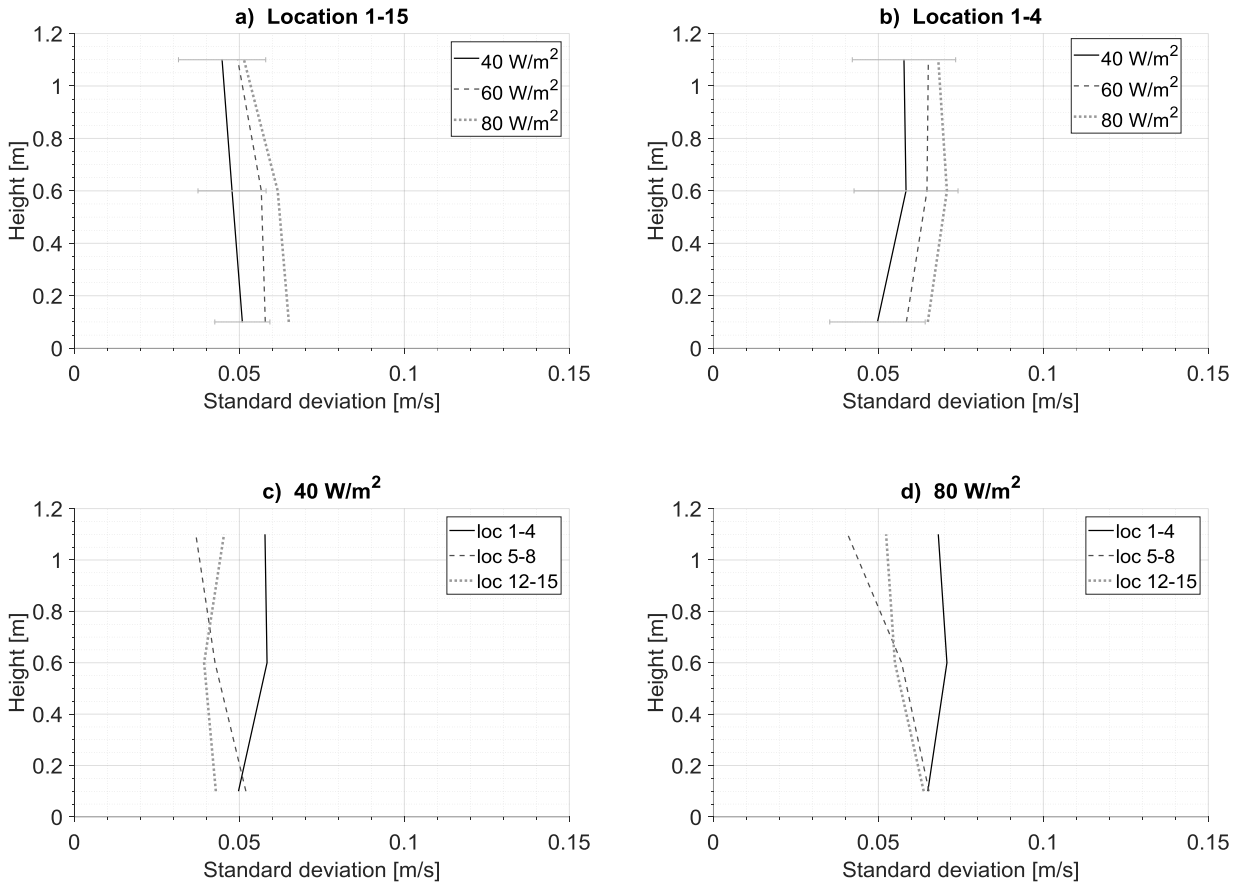

Figure 8. Standard deviation of instantaneous air speed records (1 h) as a function of room height in the seated person zone at the heat load of 40-80 W/m^2: a) Arithmetic average of measured locations 1-15 and ±standard deviation at 40 W/m^2. b) Arithmetic average of locations 1-4, i.e. at the corridor side, and ±uncertainty of measurement at 40 W/m^2 defined by Eq. (11). c) The standard deviation at the corridor side (loc. 1-4), in the middle (loc. 5-8) and at the window side (loc.12-15) in the case of 40 W/m^2 and d) in the case of 80 W/m^2.

The average air speed fluctuation of 0.06 m/s decreased by 16 % down to 0.05 m/s from the height of 0.1 m up to 1.1 m. In the symmetrical set-up [32], the standard deviation levels were greater from the height of 0.1 m up to 1.1 m. However, those differences were within uncertainty of measurement (±0.02 m/s).

In the case of 40 W/m^2, the average standard deviation of 0.04 m/s at the window side increased by 30 % up to 0.06 m/s at the corridor-side when the seated person zone was investigated. This indicates smaller air speed fluctuation near the heat sources than in the other side of the room. In the case of 80 W/m^2, the standard deviation of 0.06 m/s at the window side increased by 19 % up to 0.07 m/s at the corridor side, correspondingly. This indicates larger air speed fluctuation, but smaller relative effect at higher heat load.

At the corridor side (locations 1-4), the average standard deviation of 0.06 m/s increased by 23 % up to 0.07 m/s from 40 W/m^2 to 80 W/m^2. At the window side (locations 12-15), the corresponding deviation of 0.04 m/s increased on average by 34 % up to 0.06 m/s. This indicates higher fluctuation in the corridor side than in the window side near the workstations.

3.6 Turbulent kinetic energy

Figure 9 shows the increase of fluctuation energy defined by Eq. (5) and turbulent kinetic energy defined by Eq. (3) in the seated person zone. The diagrams in Figure 9a-b show the logarithmic presentation and the diagrams in Figure 9c-d show the mean values towards a room height. The Figure 9a-b shows a fluctuation energy as a function of frequency up to 5 Hz, i.e. half of a sampling rate due to the Nyqvist frequency [44]. The dashed line describes the Kolmogorov -5/3 law for the cascading process in turbulence. The Figure 9a-b shows that the frequency distribution follows reasonably the Kolmogorov law.

In the seated person zone, the arithmetic average of turbulent kinetic energy was 1.2E−03 m^2/s^2 in the case of 40 W/m^2. The corresponding kinetic energy was 1.8E−03 m^2/s^2 at 80 W/m^2, hence the average kinetic energy increased by 53 % from 40 W/m^2 to 80 W/m^2. The relative effect of increased heat load was thereby greater than with the standard deviation, mean air speed or turbulence intensity, similarly than in the symmetrical heat load set-up [32]. However, the average turbulent kinetic energy and the relative difference were higher in the symmetrical set-up than in the asymmetrical set-up.

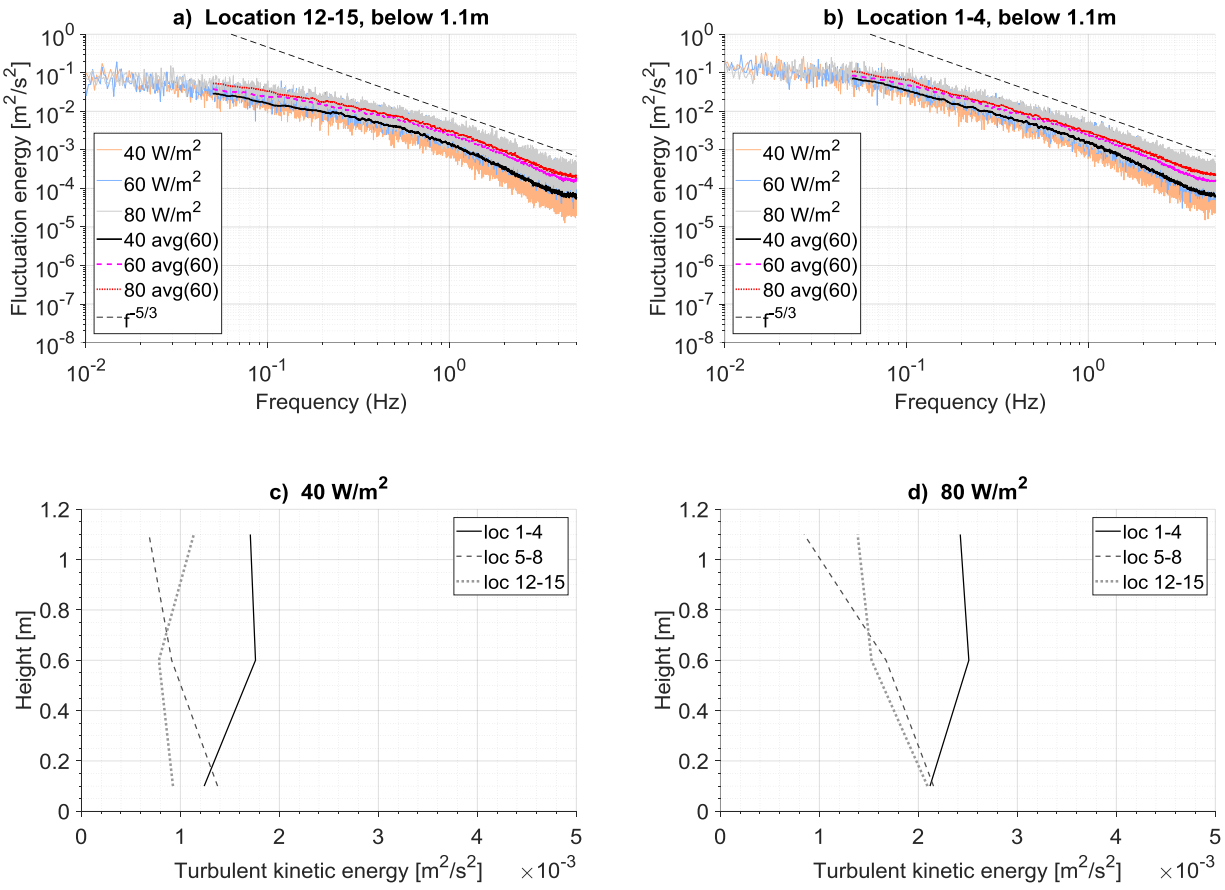

Figure 9. Turbulent kinetic energy as a function of room height in the seated person zone at the heat load of 40-80 W/m²: a) A logarithmic presentation of fluctuation energy at the window side as a function of frequency and b) a corresponding fluctuation energy at the corridor side. c) Turbulent kinetic energy at the corridor side (loc. 1-4), in the middle (loc. 5-8) and at the window side (loc.12-15) in the case of 40 W/m² and d) in the case of 80 W/m².

In the seated person zone, the average turbulent kinetic energy of 1.7E-03 m^2/s^2 decreased by 26 % down to 1.3E-03 m^2/s^2 from the height of 0.1 m up to 1.1 m. In the symmetrical set-up [32], the average turbulent kinetic energy was greater, but the relative difference between those heights was at the same level than in the asymmetrical set-up.

In the case of 40 W/m^2, the average turbulent kinetic energy of 9.5E-04 m^2/s^2 at the window side increased by 65 % up to 1.6E-03 m^2/s^2 at the corridor-side when the seated person zone was investigated. This indicates significantly smaller turbulent kinetic energy near the heat sources than in the other side of the room. In the case of 80 W/m^2, the turbulent kinetic energy of 1.7E-03 m^2/s^2

at the window side increased by 41 % up to 2.4E-03 m^2/s^2 at the corridor side correspondingly. This indicates larger fluctuation energy level, but smaller relative effect at higher heat load.

At the corridor side (locations 1-4), the average turbulent kinetic energy of 1.6E-03 m^2/s^2 increased by 50 % up to 2.4E-03 m^2/s^2 while the heat load was increased from 40 W/m^2 to 80 W/m^2. At the window side (locations 12-15), the corresponding kinetic energy of 9.5E-04 m^2/s^2 increased by 76 % up to 1.7E-03 m^2/s^2. This indicates higher relative effect in the window side near the workstations than in the corridor side.

3.7 Fluctuation energy ratio

Figure 10 shows the fluctuation energy ratio defined by Eq. (6) with the heat load in the seated person zone. In this zone, the arithmetic average of fluctuation energy ratio was 0.17 in the case of 40 W/m^2 and 80 W/m^2. This indicates that the heat load change had only a minor effect on the fluctuation energy ratio. The amount of fluctuation energy ranged from 3.3 % to 42 % in the airflow motions in the seated person zone. In the symmetrical set-up [32], the corresponding ratio was slightly greater in the seated person zone, but the range was smaller than in the asymmetrical set-up.

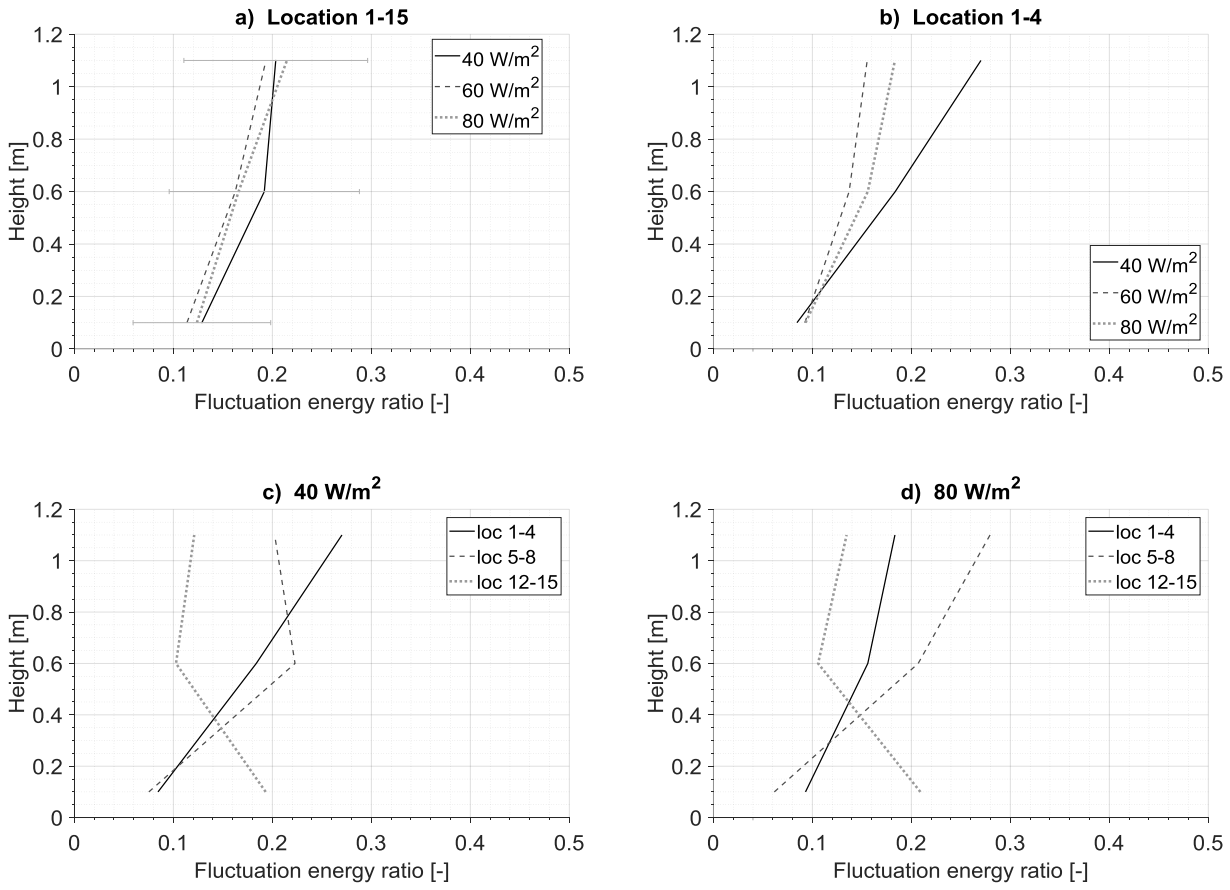

Figure 10. Fluctuation energy ratio as a function of room height in the seated person zone at the heat load of 40-80 W/m^2: a) Arithmetic average of measured locations 1-15 and ±standard deviation at 40 W/m^2. b) Arithmetic average of locations 1-4, i.e. at the corridor side. c) The fluctuation energy ratio at the corridor side (loc. 1-4), in the middle (loc. 5-8) and at the window side (loc.12-15) in the case of 40 W/m^2 and d) in the case of 80 W/m^2.

In the seated person zone, the average fluctuation energy ratio of 0.12 at the height of 0.1 m increased by 67 % up to 0.20 at the height of 1.1 m, probably due to lower mean air speed at 1.1 m. In the symmetrical set-up [32], the corresponding energy ratio was slightly greater at those heights.

In the case of 40 W/m^2, the average fluctuation energy ratio of 0.14 at the window side increased by 29 % up to 0.18 at the corridor-side when the seated person zone was investigated. This indicates slightly larger amount of fluctuation energy at the corridor side than in the window side

near the workstations. In the case of 80 W/m^2, the fluctuation energy ratio was 0.15 and 0.14, respectively. This indicates only minor difference between both sides at the higher heat load.

At the corridor side (locations 1-4), the average fluctuation energy ratio of 0.18 decreased by 20 % down to 0.14 while the heat load was increased from 40 W/m^2 to 80 W/m^2. At the window side (locations 12-15), the corresponding ratio was at the same level of 0.14 and 0.15, respectively. This indicates a small effect of heat load on the fluctuation energy ratio.

The results follow closely the corresponding symmetrical heat load results [32] in the seated person zone, in which the greater effect was obtained with the mean air speed level than with the heat load level on the fluctuation energy ratio.

3.8 On scales in airflow field

The largest length-scale was estimated to be on the order of the room size. The smallest length-scale, i.e. the Kolmogorov length-scale, was on average 4.3 mm and 3.7 mm at 40 W/m^2 and at 80 W/m^2 in the seated person zone, respectively. Hence, the smallest length-scale decreased by 15% from 40 W/m^2 to 80 W/m^2, thus producing a wider variety of eddies in the zone. Figure 11 shows the arithmetic average of the Kolmogorov length and time scales in the seated person zone.

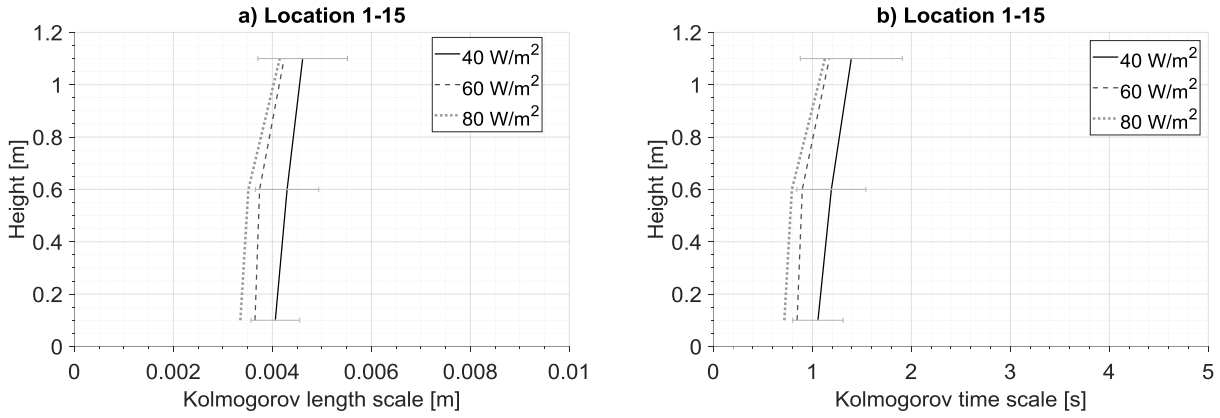

Figure 11. Arithmetic average of the a) Kolmogorov length scale and b) Kolmogorov time scale at the heat load of 40-80 W/m^2. The errorbars denote ±standard deviation at 40 W/m^2.

In contrast, both the largest time-scale and the smallest time-scale decreased towards increasing heat load. In the seated person zone, the largest time-scale was on average 30 s and the smallest time-scale was on average 1.2 s at the heat load of 40 W/m^2 when the length scale was the room height 3 m. The corresponding time-scale was 24 s and 0.9 s at 80 W/m^2, respectively. Hence, a range of time-scales decreased from 40 W/m^2 to 80 W/m^2. This means that an eddy turn-over time will decrease when the heat load and the supply airflow rate increase. Furthermore, the result indicates higher turnaround velocity and fluctuation in the flow with smaller time-scales. In the symmetrical heat load distribution [32], the time-scales were smaller than in the current study.

3.9 Large-scale circulating airflow pattern

Figure 12 idealize the large-scale circulating airflow pattern that was observed with the asymmetrical heat load distribution by using the marker smoke visualization and the anemometers. Generally, the heated buoyancy flows rose upwards and turned to flow along the ceiling surface from where the released smoke directed downwards to the opposite side of the room. The largest length scales were on the order of the room size whereas the smallest length scales were on the order of millimeters, thus the length scales were consistent with the earlier studies [25], [45].

Figure 12. Large-scale circulating airflow pattern observed in the test room.

3.10 Averaged airflow characteristics

Table 3 summarizes the time-averaged flow field over the measured locations against the thermal load and the room height. The results show e.g. that the mean air speed was higher near the floor at the height of 0.1 m than near the head level of a seated person at the height of 1.1 m. Furthermore, Table 3 shows a relative difference between the window side and the corridor side (column ΔW) in the case of 40 W/m^2. In addition, Table 3 shows the relative effect towards the increased heat load (column ΔQ) and towards the increased height (column ΔH) from 0.1 m up to 1.1 m in the seated person zone.

Table 3. The average of variable at locations 1-15 against the internal heat load and the room height. Column ΔQ refers to relative difference from 40 W/m^2 to 80 W/m^2 in the seated person zone. Column ΔH refers to relative difference from 0.1 m to 1.1 m. Column ΔW refers to relative difference from the window side to the corridor side in the seated person zone at 40 W/m^2.

Room height [m]	*0.1*	*0.6*	*1.1*	*0.1*	*0.6*	*1.1*	*0.1*	*0.6*	*1.1*	*ΔQ*	*ΔH*	*ΔW*
Heat load [W/m^2]	*40*	*40*	*40*	*57*	*57*	*57*	*80*	*80*	*80*	*[%]*	*[%]*	*[%]*
mean air speed [m/s]	0.15	0.11	0.10	0.19	0.14	0.11	0.21	0.15	0.11	32	−42	20
std. deviation [m/s] x10^{-2}	5.1	4.8	4.5	5.8	5.7	5.0	6.5	6.2	5.1	24	−16	30
turbulence intensity [%]	37	48	50	35	44	49	36	44	52	−3	39	16
draught rate [%]	10.2	6.7	5.5	12.7	9.4	6.7	14.1	10.4	6.6	39	−49	40
fluctuation energy ratio [-]	0.13	0.19	0.20	0.11	0.16	0.19	0.12	0.17	0.21	−4	67	29
tkin. energy [m^2/s^2]x10^{-3}	1.3	1.2	1.1	1.7	1.6	1.3	2.1	1.9	1.4	53	−26	65
dissipation [m^2/s^3]x10^{-5}	1.7	1.5	1.3	2.3	2.3	1.7	3.3	2.9	2.0	85	−31	104
small length scale [mm]	4.1	4.3	4.6	3.6	3.7	4.2	3.4	3.5	4.1	−15	18	−19
large time scale [s], l=3m	23	31	36	18	24	32	17	22	34	−18	77	−10
small time scale [s]	1.1	1.2	1.4	0.8	0.9	1.2	0.7	0.8	1.1	−28	41	−34

4 Discussion

The airflow characteristics were studied with an asymmetrical heat load distribution in a simplified thermal environment. The diffuse ceiling ventilation was chosen to generate cooling power, because it provides stable and low-momentum supply air distribution that may have only a little effect on the buoyancy flows from heat sources. However, the airflow characteristics are valid only with the given experimental set-up, and therefore, further studies are recommended with advanced ventilation systems and heat load layouts for improving modern indoor environments.

The airflow characteristics were studied in a wider sense than by investigating the common airflow characteristics such that the air temperature, air velocity and turbulence intensity. The discussed airflow characteristics include also turbulent kinetic energy and fluctuation energy ratio. Those are closely related to the instantaneous air speed fluctuations that were detected by using omnidirectional anemometers. Consequently, the airflow characteristics form a physical basis for exploring airflow conditions e.g. when optimizing indoor environment. Furthermore, the Fourier transform provided knowledge on fluctuation in a frequency domain.

The airflow characteristics were in a good agreement with the symmetrical heat load study [32]. Those results complement each other and evidence on average effects in airflow field at increased heat load. Both studies show that the mean air speed and the fluctuation increase with the combined effect of heat load and supply airflow rate. Furthermore, the increased heat load had only a minor effect on the turbulence intensity and the fluctuation energy ratio. The asymmetrical results differs from the symmetrical results such that the significant relative differences (>20%) were found between the heated window side and the other side of the room. This agrees with the discussion in the earlier studies [21] - [22]. In the asymmetrical study, the vertical gradient of mean air speed occurred not only near the floor but also near the ceiling zone, most probably due to large-scale circulating airflow pattern from the heat sources to the other side of the room. A large-scale circulating airflow pattern was observed by using a marker-smoke visualization that

complements the measured instantaneous data-set records of 1 h interval. The results indicate that circulating airflow pattern increases the draught rate at the ankle height of individuals.

Mustakallio et al. [33] found rather similar air speed and draught rate levels with several advanced cooling systems in a double office layout. The diffuse ceiling ventilation produced mainly slightly larger range of air temperatures at 40 W/m^2 and slightly smaller range of air temperatures at 60 W/m^2 than the CCMV, CBR and MVRC systems. However, the air temperature and the air speed levels were reasonable in all those test cases and the differences between the methods were mainly within the uncertainty of measurements. However, at 26°C air temperature levels, people may require air movement to improve satisfaction with thermal environment. Furthermore, the thermal radiation from heat sources affects the satisfaction. Thus, a sensation is most probably warmer near a heat source than further away from the source. In the current study, the amount of fluctuation energy ranged from 2 % to 42 % in the airflow motions. This may indicate laminar and turbulent regions that can be in a transitional state, which in turn agree the earlier study by Kandzia and Müller [46].

A risk of discomfort can be minimized by reducing heat sources or by directing buoyancy flows into the exhaust valve at the ceiling zone. In addition, a higher room height could decrease the risk, but the cooling capacity of diffuse ceiling ventilation has been shown to reduce with higher room height [11]. One system could be a perimeter chilled beam installation with a ceiling opening and plenum cavity for the buoyancy flows, e.g. near the windows [47].

The results indicate that diffuse ceiling ventilation could be an appropriate air distribution method also for high heat loads, because the air temperature and the air speed were reasonable, and the draught rate was moderate, i.e. mainly in the category B defined by the European Standard EN ISO 7730:2005 [19], although the airflow motion increased significantly at 80 W/m^2. This agrees with the results by Nielsen et al. [11] who concluded that supply airflow is not a large source of draught with diffuse ceiling ventilation. Consequently, most probable draught risk comes from convection flows from heat sources.

5 Conclusions

The maximum draught rate was 18-21 % indicating the category B-C of thermal environment defined by the European Standard EN ISO 7730:2005. Hence, the thermal conditions at the investigated heat loads of 40-80 W/floor-m^2 were not able to fulfill the category A.

The airflow conditions were different between the heated window side and the corridor side due to asymmetrical set-up of heat sources. The asymmetrical heat load created a large-scale circulating airflow pattern from the heat sources to the other side of the room. Consequently, the average air speed and the draught rate were higher in the corridor side than in the heated window side.

The results indicate that the mean air speed and the instantaneous air speed fluctuation increased with the heat load and the supply airflow rate. Consequently, also the turbulent kinetic energy and the turbulence dissipation increased. This may affect the satisfaction with thermal environment.

The heat load level had a small effect on the turbulence intensity, probably because both the mean air speed and the standard deviation of air speeds increased with the heat load and the supply airflow rate. Therefore, the draught rate increased significantly with mean air speed. In this sense, the increasing heat load had also a small effect on the amount of fluctuation energy over the inertial energy in the airflow motions.

The results indicate that a range of turbulent length scales increases with the heat load and the supply airflow rate. The largest length scales were on the order of the room size whereas the smallest length scales were on the order of millimeters.

The time-scales indicate a decreasing turn-over time for eddies when the heat load increases. However, the average mean air speeds were rather low in the test room. Therefore, the largest time scales were on the order of tens of seconds and the smallest time scales were on the order of second.

Acknowledgement

The authors wish to acknowledge Foundation LVY for financial support, Professor Arsen Melikov from the Technical University of Denmark and Professor Mats Sandberg from the University of Gävle, Sweden for discussion and comments. The authors would also like to express gratitude to Mr. Etienne Daviet from the Institute National des Sciences Appliquées in Lyon, France, for contributing to the measurements.

REFERENCES

[1] Mundt, E., Mathisen, M. H., Nielsen, P. V., & Moser, A. (2004). Ventilation effectiveness. REHVA Guidebook no. 2, Federation of European Heating and Air-conditioning Associations.

[2] Wyon, D. P. (2004). The effects of indoor air quality on performance and productivity. Indoor Air, Volume 14, Issue Supplement s7, pp. 92–101.

[3] Seppänen, O. (2008). Scientific basis for design of ventilation for health, productivity and good energy efficiency. In Proceedings of the international conference on indoor air quality and climate, Copenhagen, Denmark.

[4] Wargocki, P., & Wyon, D. P. (2017). Ten questions concerning thermal and indoor air quality effects on the performance of office work and schoolwork. Building and Environment, 112, 359-366.

[5] Haverinen-Shaughnessy, U., Shaughnessy, R. J., Cole, E. C., Toyinbo, O., & Moschandreas, D. J. (2015). An assessment of indoor environmental quality in schools and its association with health and performance. Building and Environment, 93, 35-40.

[6] Müller, D., Kandzia, C., Kosonen, R., Melikov, A. K., & Nielsen, P. V. (2013). Mixing Ventilation. Guide on mixing air distribution design. Federation of European Heating and Air-Conditioning Associations, REHVA, ISBN 978-2-930521-11-4.

[7] Heiselberg, P., Murakami, S., & Roulet, C. A. (1998). Ventilation of large spaces in buildings. Final Report IEA Annex, 26.

[8] Liddament, M. W. (ed.), et al. (1998). Energy-Efficient Ventilation of Large Enclosures. Technical Synthesis Report, International Energy Agency, IEA ECBCS Annex 26.

[9] Zhang, C., Heiselberg, P., & Nielsen, P. V. (2014). Diffuse Ceiling Ventilation-A Review. International Journal of Ventilation, 13(1), 49-63.

[10] Zhang, C., Kristensen, M. H., Jensen, J. S., Heiselberg, P. K., Jensen, R. L., & Pomianowski, M. (2016). Parametrical analysis on the diffuse ceiling ventilation by experimental and numerical studies. Energy and Buildings, 111, 87-97.

[11] Nielsen, P. V., Vilsbøll, R. W., Liu, L., & Jensen, R. L. (2017). Diffuse Ceiling Ventilation, Load Distribution and Ceiling Design. Proceedings of Healthy Buildings Europe, Lublin, Poland.

[12] Jacobs, P., van Oeffelen, E. C., & Knoll, B. (2008). Diffuse ceiling ventilation, a new concept for healthy and productive classrooms. Proceedings of Indoor Air, Paper ID: 3.

[13] Jacobs, P., & Knoll, B. (2009). Diffuse ceiling ventilation for fresh classrooms. In 30th AIVC Conference “Trends in High Performance Buildings, Berlin, Germany.

[14] Fan, J., Hviid, C. A., & Yang, H. (2013). Performance analysis of a new design of office diffuse ceiling ventilation system. Energy and Buildings, 59, 73-81.

[15] Melikov, A. K. (2016). Advanced air distribution: Improving health and comfort while reducing energy use. Indoor air, 26(1), 112-124.

[16] Lan, L., Wargocki, P., Wyon, D. P., & Lian, Z. (2011). Effects of thermal discomfort in an office on perceived air quality, SBS symptoms, physiological responses, and human performance. Indoor air, 21(5), 376-390.

[17] Kosonen, R., Ahola, M., Villberg, K., and Takki, T. (2011). Perceived IEQ conditions: why the actual percentage of dissatisfied persons is higher than standards indicate? Sick Building Syndrome, Springer Berlin Heidelberg, 2011, pp. 75–88.

[18] Sakellaris, I. A., D.E. Saraga, C. Mandin, C. Roda, S. Fossati, Y. de Kluizenaar, ... and O. Hänninen. 2016. Perceived indoor environment and occupants' comfort in European "modern" office buildings: the OFFICAIR study. International journal of environmental research and public health, 13(5), 444.

[19] CEN (2005). European Standard EN ISO 7730:2005, Ergonomics of the thermal environment — Analytical determination and interpretation of thermal comfort using calculation of the PMV and PPD indices and local thermal comfort criteria. European Standard EN ISO 7730:2005(E), 3rd edition, 2005-11-15, Geneva, Switzerland.

[20] Koskela, H., Häggblom, H., Kosonen, R., & Ruponen, M. (2010). Air distribution in office environment with asymmetric workstation layout using chilled beams. Building and Environment, 45(9), 1923-1931.

[21] Kosonen, R., Saarinen, P., Koskela, H., & Hole, A. (2010). Impact of heat load location and strength on air flow pattern with a passive chilled beam system. Energy and Buildings, 42(1), 34-42.

[22] Koskela, H., Häggblom, H., Kosonen, R., & Ruponen, M. (2012). Flow pattern and thermal comfort in office environment with active chilled beams. HVAC&R Research, 18(4), 723-736.

[23] Nielsen, P. V., Restivo, A., & Whitelaw, J. H. (1979). Buoyancy-affected flows in ventilated rooms. Numerical Heat Transfer, 2(1), 115-127.

[24] Tennekes H. and Lumley J. L. (1972). A First Course in Turbulence, The MIT Press, ISBN 0 262 20019 8.

[25] Etheridge, D., & Sandberg, M. (1996). Building ventilation: theory and measurement. Chichester, UK, John Wiley & Sons, ISBN 0-471-96087-X.

[26] Pope S. B. (2000). Turbulent flows, Cornell University, Cambridge University Press, ISBN 0-521-59886-9.

[27] Townsend A. A. (1976). The Structure of Turbulent Shear Flow, 2nd edition, Cambridge University Press, ISBN 0 521 29819 9.

[28] Hanzawa, H., Melikov, A. K., & Fanger, P. O. (1987). Airflow characteristics in the occupied zone of ventilated spaces. ASHRAE Transactions, vol. 93, Part 1, No. 3045.

[29] Fanger, P. O., Melikov, A. K., Hanzawa, H., & Ring, J. (1988). Air turbulence and sensation of draught. Energy and buildings, 12(1), 21-39.

[30] Loomans, M. (1998). The measurement and simulation of indoor air flow. University of Eindhoven.

[31] Bertheussen, B., Mustakallio, P., Kosonen, R., & Melikov, A. K. (2013). Comparison of the Performance of Chilled Beam with Swirl Jet and Diffuse Ceiling Air Supply: Impact of Heat Load Distribution. Clima 2013. Paper ID: 29.

[32] Lestinen, S., Kilpeläinen, S., Kosonen, R., Jokisalo, J., Koskela, H., & Melikov, A. (2018). Flow characteristics in occupied zone – An experimental study with symmetrically located thermal plumes and low-momentum diffuse ceiling air distribution. Building and Environment, Volume 128, Pages 77–88.

[33] Mustakallio, P., Bolashikov, Z., Kostov, K., Melikov, A., & Kosonen, R. (2016). Thermal environment in simulated offices with convective and radiant cooling systems under cooling (summer) mode of operation. Building and Environment, 100, 82-91.

[34] Zukowska, D., Melikov, A., & Popiolek, Z. (2012). Impact of geometry of a sedentary occupant simulator on the generated thermal plume: Experimental investigation. HVAC&R Research, 18(4), 795-811.

[35] CEN (2001). European Standard EN ISO 7726:2001, Ergonomics of the thermal environment. Instruments for measuring physical quantities (ISO 7726:1998).

[36] Dantec Dynamics (2017). Vivo Draught 20T31. Internet reference: https://www.dantecdynamics.com/ (accessed 16.2.2018).

[37] Sensor Electronic (2017). SensoAnemo 5100SF. Internet reference: http://sensor-electronic.pl/ (accessed 16.2.2018).

[38] Gemini Data Loggers (2017). Tinytag Plus 2. Internet reference: http://www.geminidataloggers.com/data-loggers/tinytag-plus-2 (accessed 16.2.2018)

[39] MathWorks (2017). MATLAB Release Notes. Internet reference: www.mathworks.com (accessed 16.2.2018).

[40] Kolmogorov, A. N. (1941, January). The local structure of turbulence in incompressible viscous fluid for very large Reynolds numbers. In Dokl. Akad. Nauk SSSR (Vol. 30, No. 4, pp. 301-305).

[41] Wilcox, D. C. (2006). Turbulence modeling for CFD. 3rd edition, DCW industries, La Canada, California, USA, ISBN 978-1-928729-08-2.

[42] Taylor, G. I. (1935, September). Statistical theory of turbulence. In Proceedings of the Royal Society of London A: Mathematical, Physical and Engineering Sciences (Vol. 151, No. 873, pp. 421-444). The Royal Society.

[43] Melikov, A. K., Popiolek, Z., Silva, M. C. G., Care, I., & Sefker, T. (2007). Accuracy limitations for low-velocity measurements and draft assessment in rooms. HVAC&R Research, 13(6), 971-986.

[44] Koopmans, L. H. (1995). The spectral analysis of time series. Academic press. ISBN: 978-0-12-419251-5.

[45] Chen, Q., & Srebric, J. (2002). A procedure for verification, validation, and reporting of indoor environment CFD analyses. HVAC&R Research, 8(2), 201-216.

[46] Kandzia, C., & Müller, D. (2016). Flow structures and Reynolds number effects in a simplified ventilated room experiment. International Journal of Ventilation, 15(1), 31-44.

[47] Woollett, J., & Rimmer, J. (2014). Active and Passive Beam Application Design Guide. Brussels: REHVA-Federation of European Heating, Ventilation and Air Conditioning Associations.